Journal of Materials Chemistry C

Micellar-Incorporated Hydrogels with Highly Tough, Mechanoresponsive, and Self-Recovery Properties for Strain-Induced Color Sensors

Journal:	*Journal of Materials Chemistry C*
Manuscript ID	TC-ART-08-2018-003914.R1
Article Type:	Paper
Date Submitted by the Author:	10-Sep-2018

Complete List of Authors:	Zhang, Yanxian; University of Akron, Chemical and Biomolecular Engineering Ren, Baiping; University of Akron, Chemical and Biomolecular Engineering Yang, Fengyu; University of Akron, Chemical and Biomolecular Engineering Cai, Yongqing; University of Akron, Chemical and Biomolecular Engineering Chen, Hong; The University of Akron, Chemical and Biomolecular Engineering Wang, Ting; Southeast University, State Key Laboratory of Bioelectronics Feng, Zhangqi; Nanjing University of Science and Technology, Chemicobiology and Functional Materials Institute Tang, Jianxin; Hunan University of Technology Xu, Jianxiong; Hunan University of Technology, Hunan Key Laboratory of Green Packaging & Application of Biological Nanotechnology Zheng, Jie; University of Akron, Chemical and Biomolecular Engineering

Micellar-Incorporated Hydrogels with Highly Tough, Mechanoresponsive, and Self-Recovery Properties for Strain-Induced Color Sensors

Yanxian Zhang[1,4†], Baiping Ren[4†], Fengyu Yang[4], Yongqing Cai[4], Hong Chen[4], Ting Wang[2,4], Zhangqi Feng[3,4], Jianxin Tang[1], Jianxiong Xu[1], and Jie Zheng[4]**

[1]Hunan Key Laboratory of Biomedical Nanomaterials and Devices
College of Life Science and Chemistry
Hunan University of Technology, Zhuzhou 412007, China

[2]State Key Laboratory of Bioelectronics
Southeast University, Nanjing 210096, China

[3]School of Chemical Engineering
Nanjing University of Science and Technology, Nanjing 210094, China

[4]Department of Chemical & Biomolecular Engineering
The University of Akron, Ohio 44325, USA

† The authors contribute equally to this work

* Corresponding Authors: (J.X.) xujianxiong8411@163.com; (J. Z.) zhengj@uakron.edu

Figure of Content

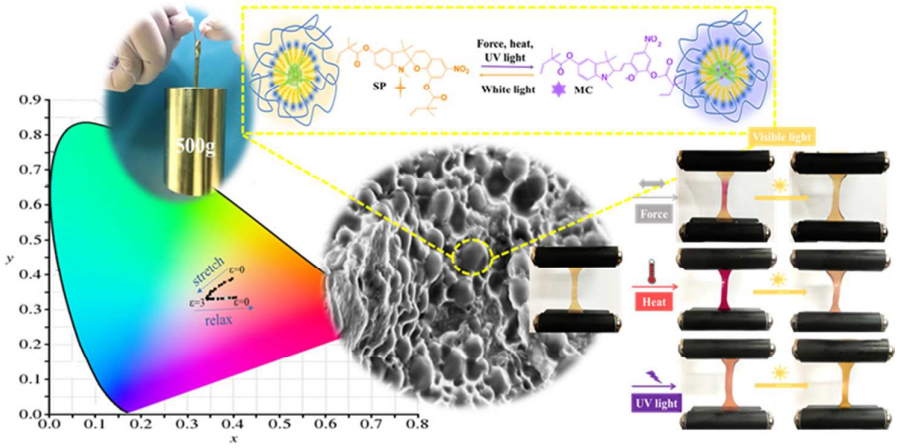

ABSTRACT

Tough, mechanoresponsive hydrogels have broad and significant impacts on fundamental research and practical applications, but have proved to extremely challenging. The poor solubility of mechanophores makes them difficult to be integrated into a highly hydrophilic network of hydrogels. In this work, we synthesized dimethylacrylate-functionalized spiropyran (SP) mechanophores and used them as crosslinkers to copolymerize with hydrophobic methyl acrylate (MA) monomers and hydrophilic N-hydroxyethyl acrylamide (AM) monomers in the presence of surfactant polysorbate 80 (TWEEEN 80) micelles, forming poly(AM-co-MA/SP) hydrogels. Mechanical properties of as-prepared and swollen poly(AM-co-MA/SP) hydrogels strongly depended on network components (AM, MA, and SP concentrations). Thus, the optimal hydrogels can achieve excellent mechanical properties (tensile stress of 1.1 MPa, tensile strain of 6 mm/mm, elastic modulus of 1.1 MPa, and tearing energy of 3200 kJ/m^2). Due to multi-stimuli-responses of SP crosslinkers, the hydrogels exhibited the reversible changes in color and mechanical properties between the force-, heat-, and UV light-induced deformation state and the white light-induced recovery state. Based on their fast, reversible, force-induced color change behavior, we further design a conceptual hydrogel strain sensor to monitor color change under the stretching and relaxing processes in multiple cycles. This work demonstrates that the presence of dynamically reversible SP crosslinkers and micellar structures are the keys to greatly enhance both mechanical and color recoverable properties of poly(AM-co-MA/SP) hydrogels, which could serve as promising smart materials for a variety of applications of soft robots, electronic skins, and strain/motion/damage sensors.

INTRODUCTION

Hydrogels as soft-wet materials contain a large amount of water (50-90%) in three-dimensional networks made of physically and/or chemically crosslinked polymers or biomolecules. Introduction of stimuli-responsive polymers, crosslinkers, and fillers into hydrogel networks will add more valuable functions for fabricating smart materials in response to light,[1,2] temperature,[3,4,5] pH,[6,7] voltage,[8,9,10] magnetic field,[11] solvent[12], and ionic strength[13,14,15]. Among them, smart mechanoresponsive hydrogels are particularly attractive because they are very promising to be used as strain/motion/damage sensors, soft electronic devices/skins, and smart robots[16-18], all of which involve similar mechanochemical processes to transduce mechanical force into a chemical, electrical, or optical signal. An intuitive design strategy for mechanoresponsive hydrogels is to integrate mechanophores into polymer networks[19], where mechanophores can be activated by two different light-responsive mechanisms of mechanochromism (i.e. visible color changes induced by mechanical force)[20] and mechanoluminescence (i.e. light emission induced by mechanical force)[21]. Obviously, mechanochromism is considered as a more convenient and effective method for directly detecting the corresponding structural/fractural changes of hydrogels without any advanced or complicated instruments.

Among different mechanophores (azobenzenes, stilbenes, spiropyrans, diarylethenes, and fulgides)[22], spiropyran (SP) particularly outperforms others for the design of novel dynamic materials because of its fast, multiple stimuli-responses to force, heat, light, solvents, redox potential, and even metal ions[20,23-25]. Under external stimuli, SP undergoes reversible structural isomerization that will induce color change between yellow at a closed-ring SP state and purple at a ring-opening merocyanine (MC) state[19,20]. The SP↔MC isomerization involves the breaking and reforming of a mechanically labile C-O bond connecting the dimethylindoline and the chromene moieties, making a fast and efficient switching between the two states. More importantly, SP mechanoactivation is mainly determined by the anchoring point of spiro C-O bonds to host polymers. In general, different anchoring points in SP need to be carefully selected on the opposite sides of spiro junction in order not to compromise the force-induced bond breaking for mechanoactivation. So, based on this design principle, three types of SP mechanophores (SP1, SP2, and SP3) have been developed and studied so far[26,27] (**Scheme 1**). The three types of SP mechanophores are distinguished from each other by different anchoring sites located at both sides of the spiro C-O bond. Specifically, SP1 locates its two anchoring sites at the aromatic rings of each side. Using SP1 as a basic motif, both SP2 and SP3 show a different anchoring site to be located at the nitrogen of dimethylindoline, and SP2 has another site same as SP1 while SP3 at a nitro-group of the aromatic ring. SP1 and SP2 are sensitive to both UV light and mechanical force due to the presence of electron withdrawing $–NO_2$ groups, while SP3 solely responds to mechanical force, not UV light. Different SP-incorporated polymers or elastomers have been developed by either polymerizing or grafting SP into polymer chains in hydrophobic or organic environments, including polytetrafluoroethylene (PTFE)[28], polyacrylates[29,30,31], polysulfones[32], polyphosphazenes[33], Pluronic[34], poly(methyl acrylate) (PMA)[20, 35], poly(methyl methacrylate) (PMMA)[24], polyurethane[23], silicone-based Sylgard 184[36], and poly(ε-caprolactone)[37], which all need to be prepared with tedious and restricted conditions

such as high pressure, high temperature, and gas environment.

However, the challenge still remains because these SP mechanophores are very hydrophobic molecules, making them extremely difficult to be incorporated into a highly hydrophilic hydrogel network. So, to covalently bind SP to different polymer hydrogels, SP mechanophores need to be further functionalized with different hydrophilic groups (e.g. hydroxyl group, anhybride group, carboxylic acid group) to improve its water solubility and to realize SP-conjugated hydrogels. Schenning and the coworkers[38] incorporated spiropyran-based derivatives into acrylic acid moiety and NIPAAm to fabricate dual-responsive hydrogels and further developed dual responsive cotton fabric using the surface initiated activators regenerated by electron transfer atom transfer radical polymerization (SI-ARGET-ATRP) method. But the hydrogel was too weak to work independently without the support of cotton fabric base. Qiu et al.[39] integrated SP with dipeptides to form SP linked D-Ala–D-Ala LMWGs-based supramolecular hydrogels, which were extremely mechanically weak to bear compressive, tensile or tearing tests[40]. To improve the mechanical strength of SP-based hydrogels, Sun et al[41] synthesized SP-poly (ethylene glycol) hydrogels whose compressive stress can reach to 49.8 MPa, but no any tensile or tearing properties were presented.

All of these SP-incorporated hydrogels aforementioned achieve mechano-transduction under different external stimuli, but they are largely limited by their mechanical weakness. There was no report about SP-responsive tough hydrogels, until recently, we developed a new micellar-copolymerization method to incorporate highly hydrophobic SP1 into highly hydrated polymer network, finally fabricating polyacrylamide-co-methyl acrylate/spiropyran poly(AM-co-MA/SP) hydrogels crosslinked by SP1 mechanophores. Poly(AM-co-MA/SP) hydrogels not only exhibit thermo-, photo-, and mechano-induced color changes, but also achieve super-strong mechanical properties (tensile stress of 1.45 MPa, tensile strain of ~600%, and fracture energy of 7300 J/m^2)[27]. In this work, we synthesized and functionalized SP mechanophore with dimethylacrylate group, then used dimethylacrylated SP as a chemical crosslinker to copolymerize with methyl acrylate (MA) in the presence of TWEEN 80 aqueous solution to form MA-contained micelles, finally covalently incorporated PMA/SP-containing micelles into hydrophilic poly(acrylamide) (PAM) network, producing poly(AM-*co*-MA/SP) hydrogels. We studied not only the effects of network components on mechanical properties of as-prepared and swollen poly(AM-co-MA/SP) hydrogels, but also the new self-recovery mechanism stemmed from both micellar structure and the light-, heat-, UV-induced reversible SP↔MC reaction. Complement to force-induced color/mechanical changes in our previous work, we also studied the UV- and heat-induced color/mechanical changes, which can also be recovered by white light. In addition, we used poly(AM-co-MA/SP) hydrogels to proof-design a strain sensor to monitor color change. It should be noted that SP-incorporated materials are highly hydrophobic including SP-polymers, SP-elastomers, or SP-organogels, thus containing no water. These SP-incorporated materials also require much higher SP concentration (1~2 mol%)[42-43] and large deformation (beyond yielding point) to activate SP conversion[20]. Also, the methods used to prepare these hydrophobic SP-incorporated are ATRP or RAFT with tedious and restricted

conditions such as high pressure, high temperature, and gas environment. Different from these hydrophobic SP-incorporated materials, our poly(AM-*co*-MA/SP) hydrogels prepared by a simple one-pot polymerization method only contained 0.2~0.3 mol% of SP to sufficiently endow the strain-induced color sensing property. Considering the 6-step SP synthesis is very complicated, we also provided a step-by-step characterization for every-step synthesis for helping other researchers. Complement to our previous study, this work provides a more complete view for the better design and understanding of new SP-based tough hydrogels for mechanochemical applications.

METHOD AND MATERIALS

Synthesis and characterization of functionalized spiropyran (SP) crosslinker

The mechanophore SP and the functionalized SP crosslinker can be synthesized according to literature procedures[20, 44]. All intermediate products were characterized by ^{1}H NMR spectrum (**Fig. S1-S5**), while final product of SP crosslinkers were systemically characterized by ^{1}H NMR, ^{13}C NMR, and HRMS spectrum (**Fig. S6-S8**).

*Compound **1** (5-methoxy-2,3,3-trimethyl-3H-indole)*

(4-Methoxy)-phenyl hydrazine hydrochloride (17.46g, 0.1 mol, 1 equiv) and methyl isopropyl ketone (MIPK) (10.78 mL, 0.1 mol, 1 equiv) were dissolved in absolute ethanol (500 mL), and sealed in a 1000 mL round-bottom flask (RBF). After purging with nitrogen gas for 10 min to eliminate the oxygen in the whole system, the reactants were stirred at 100 °C and refluxed under N_2 pressure for 5.5-8.5 h. The reaction progress was determined by TLC R_f =0.1 (1:3 v/v EtOAc/Hexane, UV). After slightly concentrating the solution under vacuum, adding silica gel (Davisil Grade 636, pore size 60 Å, 35-60 mesh particle size) and further concentrating for the following dry loading column chromatography. Compound **1** was obtained (13.06 g, 69 mmol, 69%) after column chromatography by eluting with Hexane/EtOAc gradient elution (1:0 to 3:1 to 2:1 v/v Hexane: EtOAc). ^{1}H NMR (300 MHz, $CDCl_3$): **δ** 7.45 (d, *J* = 7.9 Hz, 1H), 6.84 (dd, *J* = 2.9, 0.5 Hz, 1H), 6.82 (dd, *J* = 8.4, 2.7 Hz, 1H), 3.84 (s, 3H), 1.29 (s, 6H).

*Compound **2** (5-hydroxy-2,3,3-trimethyl-3H-indole)*

5-methoxy-2,3,3-trimethyl-3*H*-indole (**1**) (13.06 g, 69 mmol, 1 equiv) was dissolved in HBr (240 mL, 48wt%, 2.1 mol, 30 equiv). After being stirred and refluxed at 140 °C for 2 h (monitored by TLC R_f=0.35, 1:3 v/v EtOAc/Hexane, UV), the reaction mixture was cooled to ambient temperature and neutralized by saturated sodium carbonate solution. DCM (100 mL × 3) was added into the solution, the organic layer was extracted and washed with brine for further purification. The collected solution was dried by Na_2SO_4 solids overnight. After filtering and washing the Na_2SO_4 solids with DCM, the compound **2** was yield (11 g, 63.5 mmol, 92%) as brown solid under vacuum concentration. ^{1}H NMR (300 MHz, $CDCl_3$): **δ** 7.38 (d, *J* = 9.0 Hz, 1H), 6.81 (d, J = 2.4 Hz, 1H), 6.76 (dd, *J* = 7.8, 2.4 Hz, 1H), 6.34 (br, 1H), 2.26 (s, 3H), 1.30 (s, 6H).

*Compound **3** (5-hydroxy-1,2,3,3-trimethyl-3H-indolium iodide)*

5-hydroxy-2,3,3-trimethyl-3*H*-indole (**2**) (11 g, 63.5 mmol, 1 equiv) and methyl iodide (1.27 mol, 80 mL, 20 equiv) were added to a RBF, purged with nitrogen for 10 min to eliminate the oxygen, and refluxed under N_2 pressure. After stirring the mixture overnight at 40 °C (monitored by TLC, R_f =0.01, 1:2 v/v EtOAc/Hexane, UV), filtered the solids out, and washed with benzene for several times. Collected the as washed solids, recrystallized with hot ethanol to get the dark red color solvent and brown crystal. Repeated the crystallization from the solvent to get the compound **3** (16.9 g, 53.4 mmol, 84%) as the brown crystal. ^{1}H NMR (300 MHz, D6-DMSO): **δ** 10.24 (s, 1H), 7.66 (d, *J* = 8.5 Hz, 1H), 7.11 (d, *J* = 2 Hz, 1H), 6.92 (dd, *J* = 8.6, 2.2 Hz), 3.87 (s, 3H), 2.64 (s, 3H), 1.44 (s, 6H).

*Compound **4** (2-hydroxy-3-methoxy-5-nitro-benzaldehyde)*

To a 1000 mL RBF, o-vanillin (30 g, 197 mmol, 1 equiv), 150 mL glacial acetic acid and 10 mL DI water were added and cooled to 0 °C in an ice bath. Nitric acid (13.7 mL, 217 mmol, 1.1 equiv) was diluted with 150 mL glacial acetic acid and added into the reaction mixture drop wisely. During dripping nitric acid slowly, orange precipitates came out, and diluted the reaction mixture with additional glacial acetic acid when its too viscous to stir. The solution was stirred and reacted at room temperature for 2 h (monitored by TLC, R_f=0.78 (o-vanillin R_f=0.8), 0.5% MeOH/CH_2Cl_2, UV). After diluting the reaction mixture with DI water, the solids were filtered out and washed with DI water to yield yellow compound **4** (34.5 g, 175 mmol, 89%) after dried under vacuum. ^{1}H NMR (300 MHz, $CDCl_3$): **δ** 11.74 (s, 1H), 10.01 (s, 1H), 8.24 (d, *J* = 2.6 Hz, 1H), 7.95 (d, *J* = 2.3 Hz, 1H), 4.04 (s, 3H).

*Compound **5** (2,3-dihydroxy-5-nitro-benzaldehyde)*

To a 1000 mL RBF, 2-hydroxy-3-methoxy-5-nitro-benzaldehyde (**4**) (34.5 g, 175 mmol, 1 equiv) was dissolved in HBr (594 mL, 48wt%, 5.25 mol, 30 equiv). Fitted the RBF with a reflux condenser and kept reacting for 4~5 h at 140 °C hot oil bath. The reaction progress was determined by TLC R_f =0.48 (0.5% MeOH/CH_2Cl_2, UV). After cooling down at ambient temperature, diluted the solution with cold DI water and kept cooling down to 0 °C in an ice bath. The precipitates were filtered out and collected for further recrystallization. To extract the remaining products in the liquid mixture, the mixture was separated by 1:1 v/v EtOAc/CH_2Cl_2 and the organic layer was dried by Na_2SO_4 solids overnight. The Na_2SO_4 solids were filtered out and yellow solids were collected after concentration under vacuum. After gathering the solids with the precipitates from former steps and recrystallizing in boiling EtOAc, the needle shaped yellow crystals were slightly washed with cold diethyl ether to yield compound **5** (20.5 g, 112 mmol, 64%). ^{1}H NMR (300 MHz, Acetone): **δ** 10.23 (s, 1H), 8.30 (d, *J* = 2.6 Hz, 1H), 7.93 (d, *J* = 2.9 Hz, 1H), 2.81 (s, 2H).

*Compound **6** (1',3',3'-trimethyl-6-nitrospiro[chromene-2,2'-indoline]-5',8-diyl bis(2-methylacrylate))*

5-hydroxy-1,2,3,3-trimethyl-3*H*-indolium iodide (**3**) (15.9 g, 50 mmol, 1 equiv), 2,3-dihydroxy-5-nitro-benzaldehyde (**5**) (9.2 g, 50 mmol, 1 equiv), and piperidine (9.8 mL, 100 mmol, 2 equiv) were added into 500 mL absolute EtOH. The reaction mixture was heated up to 100 °C in oil bath and fitted with a reflux condenser to react for 2 h. After

cooling down to ambient temperature, filtered the precipitate out and washed with small amount of cold EtOH to get black powder. To further functionalize the compound with methylacryloyl ester group, added the black powder (17.7 g, 50 mmol, 1 equiv) and Et_3N (14.5 mL, 105 mmol, 2.1 equiv) to a 100 mL RBF, and 800 mL anhydrous THF was added to dissolve the reaction mixture. Cooled down the mixture to 0 °C in an ice bath, fluxed with nitrogen flow and protected under N_2. At the same time, methyacryloyl chloride (10 mL, 105 mmol, 2.1 equiv) was diluted with 140 mL anhydrous THF and added dropwise into the RBF. Keep stirring the reaction mixture for 16 h (monitored by TLC, R_f=0.57, 1% MeOH / CH_2Cl_2, UV) at 0 °C under N_2 pressure. After warming up the reaction mixture to ambient temperature, the solution was diluted with 200 mL diethyl ether and then filtered the precipitates out. Concentrated the solution under vacuum to get purple solids. Small amount of hexane was then added to the solids, and after stirring constantly yellow precipitates came out. The precipitates and hexane were collected and heated to boiling, and the final product compound **6** (2.6 g, 5.3 mmol, 11%) was yield as orange crystals after recrystallization.
^{1}H NMR (300 MHz, $CDCl_3$): **δ** 7.97 (d, *J* = 2.6 Hz, 1H), 7.92 (d, *J* = 2.6 Hz, 1H), 7.00 (d, *J* = 10.5 Hz, 1H), 6.87 (dd, *J* = 8.3, 2.2 Hz, 1H), 6.80 (d, *J* = 2.6 Hz, 1H), 6.47 (d, *J* = 8.2 Hz, 1H), 6.33 (s, 1H), 5.93 (d, *J* = 3.8 Hz, 1H), 5.90 (s, 1H), 5.75 (d, *J* = 1.5 Hz, 1H), 5.52 (d, *J* = 1.2 Hz, 1H), 2.66 (s, 3H), 2.08 (s, 3H), 1.63 (m, 3H), 1.25 (s, 3H), 1.22(s, 3H).^{13}C NMR (300 MHz,
$CDCl_3$):**δ** 166.24, 165.01, 150.76, 145.02, 144.50, 140.07, 138.03, 137.19, 136.10, 134.39, 12 8.41, 127.89, 126.68, 120.80, 120.07, 119.77, 119.24, 119.06, 115.20, 107.26, 51.65, 28.78, 2 5.50, 19.49, 18.48, 17.71. HRMS (*m/z*): $[M]^+$ calcd for $C_{27}H_{26}N_2O_7$, 490.1740; found, 490.1738.

SP crosslinked hydrogel synthesis

As a highly hydrophobic mechanophore, there exists a great difficulty to incorporate SP into the highly hydrophilic hydrogels. Here we fabricated a hybrid hydrogel network with both hydrophobic and hydrophilic part by a unique micellar-copolymerization method[27]. The SP crosslinker (0.2 mol% of MA), hydrophobic white light photo-initiator (phenylbis (2,4,6 trimethylbenzoyl) phosphine oxide, PBPO, 0.2 mol% of MA) and methyl acrylate (MA, 25 wt%) were added into aqueous 1 wt% TWEEN 80 solution (50 wt%), form uniform emulsion. Then the hydrophilic acrylamide (AM, 25 wt%) monomer was dissolved into the aqueous phase of emulsion and the hydrogels were formed through the photo-initiated micellar copolymerization under white light for 2h. **Fig. 2** shows the synthetic procedure.

Mechanical tests

Tensile Tests. The hydrogels were synthesized in a 1 mm thickness mold and cut into standard shape (ASTM-638-V) with a width of 3.18 mm and gauge length of 25 mm before the test. The tensile strain (ε), tensile stress (σ), elastic modulus (E) and deformation energy (W) were measured using a uniaxial tensile tester (Instron MOD EL5567, MA) with a crosshead speed of 100 mm/min. The tensile strain was calculated by the ratio of specimen's elongation to the initial length ($\varepsilon = \Delta l/l_0$). Tensile stress was defined as the load force applied on per unit of the original specimen cross-sectional area ($\sigma = F/A_0$). The elastic

modulus was determined by the slope of the initial linear regime of the stress-strain curve, and the deformation energy was calculated from the area under the stress-strain curve.

Tearing tests. Hydrogels with 1 mm thickness, 40 mm length and 20 mm width were cut into trousers shape with an initial notch of 20 mm. Each arm of the samples were clamped and one of the clamp was pulled up at 50 mm/min speed. The tearing energy (T) is defined as the work required to tear a unit area and estimated in the test by $\mathrm{T} = 2F_{ave}/w$, where F_{ave} is the average force during steady-state tear, and w is the width of the specimen.

Hysteresis tests. The cyclic tensile tests were also conducted by the uniaxial tensile tester with a crosshead speed of 100 mm/min and a maximum tensile strain ε=3. The dimension and shape of hydrogel specimens were exactly the same with that for tensile test. And for all cycles, the strain were calculated based on the initial length of specimens. The energy dissipation (U_{hys}) during each cycle was calculated by the area between the loading and unloading cycle.

Swelling ratio

The as-prepared hydrogels were cut into small disks with a diameter of 8 mm and immersed in water for 24 h to reach an equilibrium swelling state. The weight of specimen before (w_0) and after swelling (w_s) were measured to determine its swelling ratio (q). The swelling ratio was calculated as $q= w_s/w_0$ and recorded as mean and standard deviation (n=3).

Optical color characterization

The visible color change of SP crosslinked hydrogels in response to force, heat and UV light were characterized by the digital image analysis. All the images were taken by the Nikon D7000 camera. To further balance the white background, the background of all the images were split into RGB channels and balanced to the RGB value of pure white (RGB 220, 220, 220) with the help of Image-J software. Then the corrected image can be obtained by merging the RGB channels and the RGB value of the center of specimens was obtained from the histogram of the area. To directly identify the color change in response to different external stimuli, the RGB values were converted to the (*x, y*) value and presented in the chromaticity diagram (CIE 1931 color space).

RESULTS AND DISCUSSION

Synthesis and characterization of functionalized SP crosslinker and poly(AM-co-MA/SP) hydrogels

Fig. 1 shows a general synthesis of a dimethylacrylate-functionalized SP crosslinker. Briefly, the SP crosslinker (Compound **6**) was synthesized from the Compound **3** (*5-hydroxy-1,2,3,3-trimethyl-3H-indolium iodide*) and the Compound **5** (*2,3-dihydroxy-5-nitro-benzaldehyde*) in the presence of piperidine and further functionalized with methylacryloyl ester group from the reaction with methylacryloyl chloride. Firstly, to synthesize Compound **3**, the (4-Methoxy)-phenyl hydrazine hydrochloride was reacted with methyl isopropyl ketone in the presence of ethanol, forming the intermediate product Compound **1** (*5-methoxy-2,3,3-trimethyl-3H-indole*)**.** Then the methoxy group on the benzene

structure of Compound **1** was replaced with hydroxyl by the hydroxyalkylation with HBr to form the Compound **2** (*5-hydroxy-2,3,3-trimethyl-3H-indole*)**.** The Compound **3** can be synthesized by iodization with CH_3I on the amine group. The o-vanillin was attached with a nitro-group from the reaction with HNO_3, forming the intermediate product Compound **4** (*2-hydroxy-3-methoxy-5-nitro-benzaldehyde*). Finally, the Compound **5** was synthesized after replacing the only methoxy group of Compound **4** with hydroxyl by the hydroxyalkylation with HBr. All intermediates and final product of SP were confirmed and characterized by $^1H/^{13}C$ NMR spectrum and HRMS spectrum in **Fig. S1-S8**.

Fig. 2a shows a general process for the preparation of poly(AM-co-MA/SP) hydrogels. First, to incorporate hydrophobic SP into a hydrophilic network, we proposed to introduce TWEEN 80 (1wt %) as a nonionic surfactant and emulsifier, whose inner hydrophobic pores enable to encapsulate SP and MA via hydrophobic interactions, while external hydrophilic headgroups allow to copolymerize with polymeric AM (PAM). In this way, TWEEN 80 serves as bridges to connect both hydrophobic polyMA and hydrophilic PAM to form a compatible hydrogel network. To test this design strategy, all reactants, including MA, AM monomers, white light-initiators (PBPO), TWEEN 80 (1wt%), and SP crosslinker, were dissolved in water at room temperature and formed a smooth emulsion after vortex. Then, upon white light stimuli, MA monomers were covalently crosslinked by SP to form a PMA/SP network inside of TWEEN 80 micelles. Simultaneously, AM monomers were copolymerized with MA (i.e. AM-*co*-MA copolymerization) to connect with the PMA/SP micelles, resulting in poly(AM-*co*-MA/SP) hydrogels. The as-prepared poly(AM-*co*-MA/SP) hydrogel displayed light yellow but transparency when viewed by the naked eyes, indicating that SP molecules are well dispersed in the gels. Upon freeze-dried of fully swollen poly(AM-*co*-MA/SP) hydrogel, the cross-sectional gel structures, as shown in SEM images, clearly showed the presence and dispersion of typical micelles in the PAM network (**Fig. 2b1-b2**). The micelles that were uniformly embedded in the external network displayed spherical shapes with an average size of ~5 μm. In addition, as-prepared hydrogels also showed mechanically induced reversible fluorescence changes. As shown in **Fig. 2c1 and d1,** strong black and red "cross" fluorescence symbols as caused by compression were clearly displayed in the green (filtered by green fluorescent protein) and black (filtered by Cyanine5) backgrounds, respectively. However, after exposure of the gels to white light for 1 min, the imprinted "cross" symbols disappeared rapidly (**Fig. 2c2-d2**), also indicating a quick reversible fluorescence change between force-induced deformation and white light-induced recovery states.

Mechanical properties of poly(AM-co-MA/SP) hydrogels at as-prepared and swollen states

At a first glance, poly(AM-*co*-MA/SP) hydrogels exhibited strong and flexible properties to withstand the knotted stretching up to over 10 times its initial length (**Fig. 3a**) and hold a weight of 500 g up to ~1000 times of its own weight (**Fig. 3b**) without breakage. **Fig. 3c** shows the crack propagation process of a notched poly(AM-*co*-MA/SP) hydrogel. It can be seen that the initial crack blunting tip gradually developed into a semicircular shaped crack, and the notch remained stable as the gel was stretched up to 4 mm/mm strain,

indicating the notch-insensitivity behavior of the gel. In all three tests, upon different deformations (i.e. stretching, lifting, and cracking), poly(AM-*co*-MA/SP) hydrogels not only demonstrated their highly robust and deformable properties, but also showed an obvious color change from yellow to purple at the stress-concentrated and deformed area.

To gain additional insight into the SP-induced reinforcement mechanism of poly(AM-co-MA/SP) hydrogels, we conducted a series of tensile tests to investigate the effects of network components (crosslinker, MA, and AM concentrations) on mechanical properties of poly(AM-*co*-MA/SP) hydrogels. **Fig. 4a** compared the effect of crosslinker types on tearing energy between SP crosslinked poly(AM-*co*-MA/SP) hydrogel and ethylene glycol dimethylacrylate (EGDMA)-crosslinked (poly(AM-*co*-MA/EGDMA) hydrogel. The tearing energy of poly(AM-*co*-MA/SP) hydrogel was ~3200 J/m^2, which was 5 times higher than that of poly(AM-*co*-MA/EGDMA) hydrogel (~650 J/m^2). In **Fig. 4b**, during a cyclic loading-unloading test, poly(AM-*co*-MA/SP) hydrogel (0.36 MJ/m^3) showed a much larger hysteresis loop and dissipated more energy than poly(AM-*co*-MA/EGDMA) hydrogel (0.05 MJ/m^3). Such crosslinker-induced difference in mechanical properties proves that the SP-crosslinked network provides a unique way to dissipate energy via the mechanoactivation from a SP state to a MC state, i.e. the stress transmitted across SP crosslinkers to cleave the labile spiro C-O bond allows to dissipate energy more effectively, thus improving hydrogel toughness.

Considering poly(AM-*co*-MA/SP) hydrogel contains a hybrid network made of both hydrophobic micellar-encapsulated MA/SP and hydrophilic AM chains, we further examined the dependence of MA:AM ratio and SP concentration on mechanical properties of poly(AM-*co*-MA/SP) hydrogels. In **Fig. 4c** and **Table S1**, at a low MA:AM ratio of 1:4 and a constant SP concentration of 0.2 mol%, poly(AM-*co*-MA/SP) gel was very brittle and showed a weak tensile stress (σ_f) of 0.234 MPa at a low strain (ε_f) of 0.76 mm/mm, while at high MA:AM ratio of 4:1, poly(AM-*co*-MA/SP) gel became highly ductile as evidenced by a much larger tensile strain (ε_f) of 2.45 mm/mm at the expense of tensile stress (σ_f) of 0.052 MPa. But at an optimal MA:AM ratio of 1:1, poly(AM-*co*-MA/SP) hydrogel reached the best tensile properties (E of 0.826 kPa, σ_f of 0.771 MPa, ε_f of 6.07 mm/mm and W of 2.67 MJ/m^3). In **Fig. 4d**, the increase of SP concentrations from 0.1 mol% to 0.3 mol% led to the increase of elastic modulus (E) from 0.556 KPa to 1.074 KPa, tensile stress (σ_f) from 0.271 MPa to 1.083 MPa, and deformation energy (W) from 1.12 MJ/m^3 to 3.46 MJ/m^3 at similar tensile strain (ε_f) of ~6. Such different mechanical performances of poly(AM-*co*-MA/SP) hydrogel provides some insights into its structure-property relationship, particularly related to micelle structure. In parallel, we also characterized the color change of poly(AM-*co*-MA/SP) hydrogels in response to external forces using tensile tests. In fact, external force can be calculated from the tensile stress-strain curves. To be consistent, we prepared a series of hydrogels under the same conditions used in **Fig. 4c-4d**, and then we showed the color of hydrogel strips under different external forces (**Fig. 4e-4f**) and the stress-external force curves (**Fig. S9**). As expected, as external force (i.e. tensile strain) increased, poly(AM-co-MA/SP) hydrogels exhibited higher degree of color change towards purple, indicating that more labile C-O bonds were broken and more SP molecules were transferred to MC isomers, which also

contributed to the high mechanical performance of the poly(AM-*co*-MA/SP) hydrogel.

As demonstrated in **Fig. 5**, at the lower MA:AM ratios of 1:4, the external PAM chains formed a network with extremely high density while the internal PMA/SP inside micelles was relatively loosed. Such unbalanced and highly crosslinked structure leads the PAM network to be more brittle, but has to be endured most of external force. Thus, upon deformation, the PAM network will be fractured before the force is transferred to the micelles. This also explains no color-change of the poly(AM-*co*-MA/SP) specimen with low MA:AM ratio of 1:4 even after break. Differently, for hydrogels with extremely high MA:AM ratio of 4:1, the PMA/SP density inside the micelles was high, while the PAM network was loosely entangled. Once the hydrogel was stretched, the force will be quickly transferred from the soft and ductile PAM network to the stable micelle network, thus the mobility of micellar structure and the highly crosslinked PMA/SP network contribute to a large plastic deformation, but fail at low tensile stress. Particularly, at an optimal MA/AM ratio, the inner and external polymer chains were well balanced in the hydrogel network. So upon deformation, the MA/SP-contained micellar network helps to bear stress as the PAM network is fractured due to the effective force transfer from the ductile hydrophilic PAM network and the large energy dissipation from the SP crosslinked hydrophobic network inside the micelles.

Since hydrogels are commonly used in wet environments, the swelling of hydrogels has significantly impact on their mechanical properties and other functions. The as-prepared poly(AM-co-MA/SP) gels were immersed in water for 24 h at room temperature to achieve fully swelling equilibrium. **Fig. 6** shows the effects of MA:AM ratio and SP concentration on the swelling and mechanical properties of poly(AM-*co*-MA/SP) gels. For the MA:AM ratio-induced swelling effect, **Fig. 6a1** provides a side-by-side comparison of poly(AM-*co*-MA/SP) gels at the as-prepared and the swelling states. Qualitatively, visual inspection showed that the swollen gels displayed the larger volume expansion as MA:AM concentration ratio increased. Quantitatively, the swelling profile in **Fig. 6a2** showed that all hydrogels underwent an initial fast swelling during the first 4 h, followed by a slow swelling to achieve its equilibrium swelling state at ~10 h. The increase of MA:AM ratio from 1:4 to 3:2 caused the swelling ratios to be largely reduced from ~7 to ~2.5, simply because the hydrogels with the higher AM concentration formed more dense and hydrophilic network that tends to uptake more water to fully expanse its volume. For the poly(AM-*co*-MA/SP) hydrogel with extremely high MA:AM ratio of 4:1, whose hydrophilic PAM network was too loosely entangled, and was not strong enough to keep its shape at a swelling state. In addition, further tensile tests showed that as compared to as-prepared hydrogels, swollen hydrogels can still maintain their high tensile stress of 0.07-0.38 MPa and tensile strain of 3.8-4.6 mm/mm (**Fig. 6a3**), though these values were lower than those of as-prepared gels. Similarly, poly(AM-co-MA/SP) gels also showed SP-concentration dependence on swelling behavior (**Fig. 6b1**). The increase of SP concentration from 0.1 mol% to 0.3 mol% led to the reduction of swelling ratio from ~5 to ~3.5 (**Fig. 6b2**), but the increase of tensile stress from 0.05 to 0.42 MPa (**Fig. 6b3**). With increasing SP concentration, the crosslinking density of the hydrophobic micellar network increased, which makes the network become stronger to prevent the hydrogels from swelling, resulting in the decrease of the swelling ratio and the

increase of tensile stress. Similarly, the pre-stretching resulted from swelling largely decreased elastic modulus. Overall, regardless of MA:AM ratio- or SP concentration-induced swelling, the higher swelling ratios indicate the larger volume/network expansion, which causes polymer chains to be pre-stretched and to lose the certain degree of chain flexibility. Both effects would cause stress to be less dissipated through the interaction of polymer chains during the stretching process, leading to the reduction of mechanical properties to some extents.

Light-induced mechanoresponsive properties of poly(AM-co-MA/SP) hydrogels

Due to the reversible SP↔MC conversion and dynamic micelle structure, the poly(AM-*co*-MA/SP) hydrogels are expected to possess some degree of mechanoresponsive self-recovery ability. Thus, we tested the self-recovery and energy dissipation of poly(AM-*co*-MA/SP) hydrogels using a five-cyclic loading-unloading test. For each loading-unloading cycle, the hydrogel was stretched to 300% of its initial length during the loading process, then was exposed to white light (wattage=8W) for 0, 1, 5, and 10 min for recovery during the unloading process. Force-induced and light-induced mechanical/color change and recovery were characterized by color changes (**Fig. 7a**), cyclic stress-strain tests (**Fig. 7b**), and stiffness/toughness recovery ratios (**Fig. 7c**). Visual inspection in **Fig. 7a** also showed that during the 1st cycle, the hydrogel was turned its color from yellow to purple at the stress concentrated area. Without introducing white light in the 2nd cycle, the purple still remained. Meanwhile, in **Fig. 7b**, in the 1st cycle, the as-prepared hydrogel displayed a large hysteresis loop with dissipated energy of 0.36 MJ/m^3 and elastic modulus of ~1.0 MPa, demonstrating high mechanical stress and toughness. After the first loading-unloading cycle, the second loading cycle was applied immediately to the same gel specimen without introducing any white light for recovery. The hysteresis loop in the 2nd cycle was reduced by almost 50% as evidenced by small dissipated energy of 0.18 MJ/m^3. This indicates that the first-loading-induced network fracture can not be recovered immediately without the white light-induced MC→SP recovery, resulting in very limited energy dissipation and low stiffness/toughness recovery of 31.5%/48.8% in the 2nd cycle (**Fig. 7c**). To test white-light induced MC→SP self-recovery behavior, before loading in the 3rd cycle, 1 min of white light was shed into the same gel so that the color of stress area became lightered, indicating the certain degree of the conversion from MC to SP. So, upon white-light-induced self-recovery, subsequent loading-unloading test confirmed that the dissipated energy was increased to 0.32 MJ/m^3 corresponding to 88.4% of the original hysteresis loop and the stiffness/toughness recovery was also increased to 51.8%/88.4%. In the following 4th and 5th cycles, with increase of white-light exposure time to 5 and 10 min, respectively, the gel can almost completely recover its color to original pale yellow. The stiffness/toughness recovery was also improved to 72.2%/79.2% and 68.9%/92.8%, respectively for successive 4th and 5th loading-unloading cycles. Such loading-unloading recovery can be repeated for multiple times to demonstrate reversible color and mechanical changes between the force-induced SP→MC state and white light-induced MC→SP state.

On the other hand, considering that SP was encapsulated into TWEEN 80 micelles, it is also interesting to examine whether micelle structure also plays a role in the self-recovery of

poly(AM-*co*-MA/SP) hydrogels. Here we designed the two three-cycle loading-unloading tests for the hydrogels. First, the two hydrogel specimens were tested under the exact same conditions in the first two cycles in order to obtain the same deformation state of the gels. Then in the 3rd cycle, one specimen was exposed to white light, while the other one was exposed to UV light for 10 min to distinguish the effect of the MC→SP reversion on the self-recovery efficiency. As shown in **Fig. 8a1-b1**, after the immediate 2nd cycle, both specimens showed similar cyclic stress-strain curves and stiffness/toughness recovery values of 67.0%/50.5% (**Fig. 8a2-b2**). However, in the 3rd cycle, the gel specimen – upon exposing to white light – achieved almost complete stiffness/toughness recovery of ~100%/100% (**Fig. 8a2**), while the specimen exposed to UV light had a stiffness recovery of 100%, but a smaller toughness recovery of 80% (**Fig. 8b2**). Generally speaking, during the deformation process, the mechanical force first ruptured the micelle structures and then transferred to the SP, which triggers the SP→MC reaction. Hence, during the unloading process, the self-assembled micelles and MC→SP reversion are the vital pathways for the mechanical recovery of the gels. For the recovery under UV light during the 3rd cycle, the MC→SP reversion was inhibited by UV light while the self-assembly of the micelles can still carry on due to spontaneous hydrophobic association, thus the network was partially recovered to reach toughness recovery of 80%. For the recovery under white light, MC→SP reversion was accelerated, in line with the recovery of micelle structure, so both effects contributed to ~100% of stiffness and toughness recovery. It appears that the self-assembly of micelles is critical for the mechanical recovery of poly(AM-*co*-MA/SP) hydrogels, while white-light induced MC→SP reversion provides an additional pathway to further improve the self-recovery ability of the gels.

Heat- and UV-induced mechanoresponsive properties of poly(AM-co-MA/SP) hydrogels

The labile spiro C-O of SP can be ruptured by mechanical force, UV light, and high temperature. Apart from force-induced mechanoresponsive properties, we further examined heat- and UV-induced mechanoresponsive properties of poly(AM-co-MA/SP) hydrogels. In **Fig. 9a**, visual inspection of poly(AM-*co*-MA/SP) hydrogels showed that the as-prepared gel displayed a typical yellow color at a SP state, but after the introduction of force, heating of 60 ^{o}C for 30 min, and UV light for 30 min, the gels changed its color from yellow to a purple-like color, indicating the conversion of SP to MC in the gel network. The degree of color change was slightly different under different stimuli, indicating the different sensitivity of spiro C-O bond in SP to mechanical force, high-temperature, and UV irradiation. In all three cases, upon exposure the gels to white light for 10 min, all gels at the MC state reversed its purple-like color to original pale yellow, confirming a white-light-induced color recovery from the MC to the SP state.

Quantitatively, the optical color change and recovery of the gels between deformed (MC) state and relaxed (SP) state can be analyzed by the RGB (red, green, blue) values, which were converted into the *x, y* chromaticity diagram (CIE 1931 color space) in **Fig. 9b**. Upon deformation, the gels showed a similar color change pathways towards pink color under force and temperature stimuli. However, UV-induced color change pathway was distinct from the force- and heat-induced color change pathways, i.e. both UV- and

white-light-induced color change pathways followed the SP→MC isomerization towards pink and the MC→SP isomerization towards dark yellow at the expense of blue color value, respectively. This unique color transition pathway may be due to the photoisomerization of MC influenced by high energy UV light[20].

We also compared the mechanical recovery of poly(AM-co-MA/SP) hydrogels between the stimuli-induced deformation state and the white-light-induced recovery state using the same cyclic loading-unloading tests as **Fig. 9a**. In **Fig. 10**, using the initial hysteresis loop of the as-prepared gel as a control in the 1st loading-unloading cycle (**10a**), the subsequent 2nd loading-unloading test after applying different stimuli to poly(AM-co-MA/SP) hydrogels showed different hysteresis loops as induced by force (**10b1**), heat (**10b2**), and UV (**10b3**). The stimuli-induced hysteresis loop areas were in a decrease of order of $loop_{force}$>$loop_{uv}$>$loop_{heat}$, corresponding to the dissipated energy of 0.335 MPa, 0.616 MPa, and 0.622 MPa and stiffness/toughness recovery of 37.3%/79.3%, 58.7%/97.8%, and 92.0%/98.9%, respectively. This indicates that different stimuli induce different extents of energy dissipation and network deformation. Upon introduction of white-light for recovering the three stimuli-deformed hydrogels in the 3rd cycle, the hysteresis loop became much larger for the force-induced hydrogel whose stiffness/toughness recovery increased from 37.3%/79.3% in the 2nd cycle to 95.9%/88.2% in the 3rd cycle. As compared to the force-induced hydrogel, heat-induced and UV-induced hydrogels achieved relatively low stiffness/toughness recovery of 66.7%/66.6% and 66.6%/71.2%, respectively. This different recovery performance may come from the diverse mechanism for the SP→MC reaction under force, heat and UV stimuli. For force activated SP→MC reaction, the force is transmitted to C-O bond through polymer chains to rupture the bond and convert SP to MC, which can be easily recovered upon stress and strain relaxation accelerated with white light. However, for the heat-induced SP→MC reaction, the chain mobility was increased for SP activation, and high temperature lowered the activation energy barrier to rupture the C-O bond, leading to large SP activation (as indicated in **Fig. 9b**) that also in turn increases the barrier for the reverse reaction of MC→SP. For the UV-induced SP activation, the high energy UV light can lead to the photoisomerization of both SP and MC, thus the relative low recovery of hydrogels. Thus, the mechanical recovery of poly(AM-co-MA/SP) hydrogels depends on the strength and quantity of the reversible crosslinks in polymer network.

Poly(AM-co-MA/SP) hydrogels used as strain-induced color sensors

Inspired by the force-induced color change of poly(AM-co-MA/SP) hydrogels, we further tested whether the poly(AM-co-MA/SP) hydrogel could be used as a proof-of-concept strain sensor to monitor color changes by naked eyes, which outperform the dye-based hydrogels for strain sensing[45]. Here we recorded the color changes at different strains by optical images to demonstrate poly(AM-co-MA/SP) hydrogels as strain indicator using the RGB analysis. As shown in **Fig. 11a**, after splitting the images to the RGB channels, a total scale value of each color channel can be obtained from the peak of pixel. The background color as a control was firstly white-balanced by multiplying a factor for each color channel to normalize them to white color (RGB value of 220, 220, 220). Then, the RGB values of the stressed center of the stretched/relaxed gels can be read from the histogram of the normalized

images. Finally, the RGB values were converted into (*x, y*) values in CIE *xy* chromaticity diagram. Using this color measurement protocol, **Fig. 11b** shows the (*x, y*) color values of the gels in the gauge section at different strains of ε=0-3 during stretching and relaxing process. It can be seen that the gel displayed a linear color change pathway changing from yellow to pale purple when stretching the gel from strain ε=0 to ε=3, with a linear fitting R^2 of 0.96. Then, the gel was immediately relaxed from ε=3 to ε=0, and the corresponding color change pathway changed followed a different linear pathway (R^2=0.83) from pale purple towards slightly desaturated red, which was not overlapped with the stretched pathway. While the gel indeed shows strain-dependent color changes, the different color change pathways during the stretching and relaxing processes may result from the secondary color change by the isomerization and accumulation of MC after gel relaxing. So, based on the linear correlation between strain and chromaticity (*x, y*), it is expected that for a given specific strain of the gel, its corresponding color or color change pathway could be quantitatively identified by chromaticity output of the image, and vice versa.

We also studied the color change of poly(AM-*co*-MA/SP) hydrogel as a function of different response times under the same external strain. As shown in **Fig. 12a**, the original hydrogel displayed light yellow color. When the strain reached up to ε=3, the light purple color emerged immediately, and this color remained almost unchanged even after 3 min as evidenced by chromatic values. This result indicates that the color change of hydrogel is extremely sensitive to external force with almost immediate response time, in good accordance of the mechanism of the isomerization of SP crosslinked in the poly(AM-*co*-MA/SP) hydrogel, which is valuable to be applied for instant strain color sensor. Additionally, the reversibility of this strain-induced color change is another vital factor for real-world applications. Hence, a cyclic loading-unloading test was conducted on the same hydrogel to test the repeatability of the strain-induced hydrogel as a color sensor. During the loading process, the same hydrogel was stretched to the same strain of ε=3, while during the unloading process, the hydrogel was recovered under white light for 10 min. As shown in **Fig. 12b**, the starting/ending chromatic values of 1st, 5th, 10th, and 15th cycles, and the corresponding color change pathways of poly(AM-*co*-MA/SP) hydrogel were nearly the same, clearly demonstrating that poly(AM-*co*-MA/SP) hydrogels possess excellent color reversibility that could be used as potential strain-induced color sensors. Furthermore, we examined the effect of different recovery times (0, 2, 4, 6, 8, and 10 min) on different hydrogel samples stretched at the same strain of ε=3. As shown in **Fig. S10** below, the gel can not be fully recovered to yellow color if the recovery time under white light was less than 10 min, although all time-responsive color change points were still on the same pathway (straight line) indicating a good reversibility.

The poly(AM-*co*-MA/SP) hydrogel shows immediate color change upon external force, but relatively long time of 10 min for color recovery. On the other hand, the hydrogel may give longer visible color warning for damage locations before fully recovery, which would be valuable for damage sensing/warning applications and recording the body motion. As a simple proof-of-concept, we further demonstrate the potential application of the poly(AM-co-MA/SP) hydrogel as wearable strain sensor, which would detect the simple joint

motion of the finger as shown in **Figure S11**. By firmly attaching a hydrogel stripe on the joint of the index finger, even with a simple bending motion, hydrogel stripe detected such minor stretching and changed its color from yellow to purple, which could be used for identifying the damage/deformation location of the body. Similarly, this hydrogel could also be applied for the detection of the structural-based deformation of facilities such as pipes, shelves, and supporting structures. Using the unique mechano-responsive property of the poly(AM-co-MA/SP) hydrogels, we demonstrate a proof-of-concept example for a strain-induced color sensor based on the simple image capture and processing method.

CONCLUSIONS

Development of tough, mechanoresponsive hydrogels is a promising yet challenging task for smart materials and their relevant applications. Herein, we developed a facile micellar copolymerization method to synthesize poly(AM-co-MA/SP) hydrogels, in which Tween80 micelles served as bridges to connect a hydrophobic poly(MA/SP) network inside Tween80 with a hydrophilic polyAM network outside Tween80. Collective mechanical data from the tensile stress-strain, tearing, cyclic loading-unloading tests demonstrated that the poly(AM-co-MA/SP) hydrogels exhibited excellent mechanical properties (σ_f of 1.1 MPa, ε_f of 6 mm/mm, E of 1.1 MPa, W of 3.5 MJ/m^3, and tearing energies of 3200 J/m^2) by tuning the concentration of network components (i.e. MA, AM, and crosslinker). Based on reversible SP↔MC crosslinkings in the network, poly(AM-co-MA/SP) hydrogels also displayed reversible changes in color and mechanical properties between force-/heat-/UV-induced deformable network and white light-induced recoverable network. Poly(AM-co-MA/SP) hydrogel can almost completely recover its stiffness and toughness after 10 min resting under white light. Such high mechanical and self-recoverable properties are mainly attributed to the effective energy dissipation through the reversible labile C-O bonds in SP and (re)self-assembly of micelle structures. Additionally, as a proof-of-concept, we used the mechano-responsive property of poly(AM-co-MA/SP) hydrogel to demonstrate that the gel could be used as the strain-induced color sensor. This work offers a new strategy to incorporate hydrophobic SP mechanophores into the gel network for fabricating tough and mechanoresponsive hydrogels, which would be highly useful in wearable soft sensors and devices with programmable and versatile properties.

Acknowledgement. J.Z. thanks financial supports from NSF (DMR-1607475 and CMMI-1825122). J.T. thanks financial support from the National Natural Science Foundation of China (51774128).

Scheme 1. Three types of SP mechanophores distinguished from their anchoring groups for different functionalization and applications.

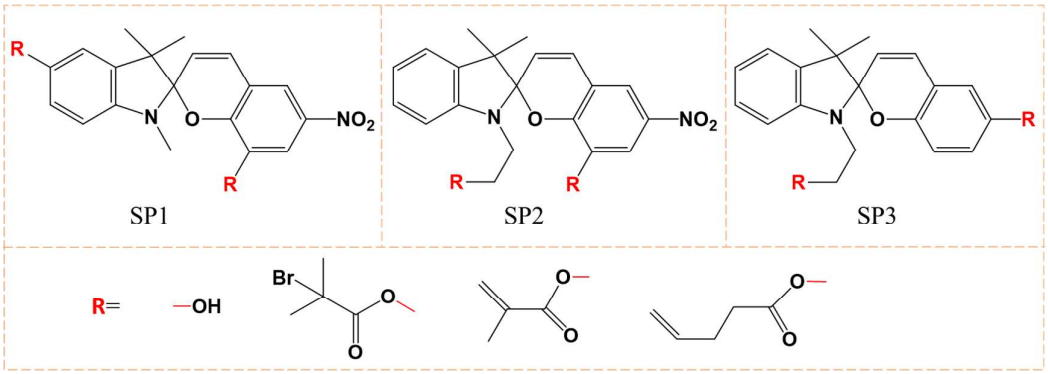

Figure 1. Synthesis routine for a functionalized SP crosslinker.

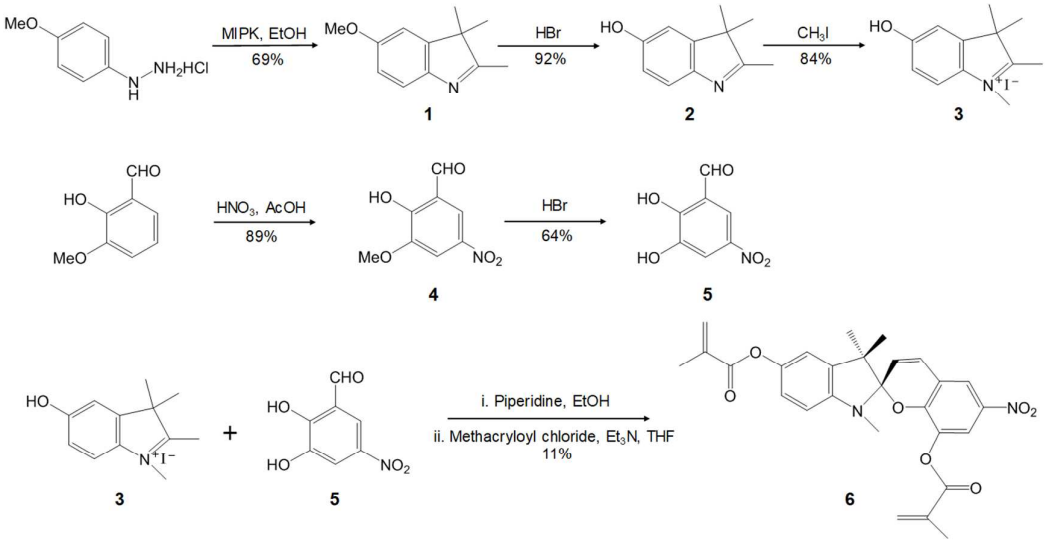

Figure 2. (a) Synthesis of poly(AM-*co*-MA/SP) hydrogels. (b1,b2) SEM image of poly(AM-*co*-MA/SP) hydrogel with micellar structure at different scale. And the reversible mechanically induced fluorescence observed under GFP filter (c1,c2) and Cy5 filter (d1,d2), as indicated by the emergence and disappearance of "X" imprint.

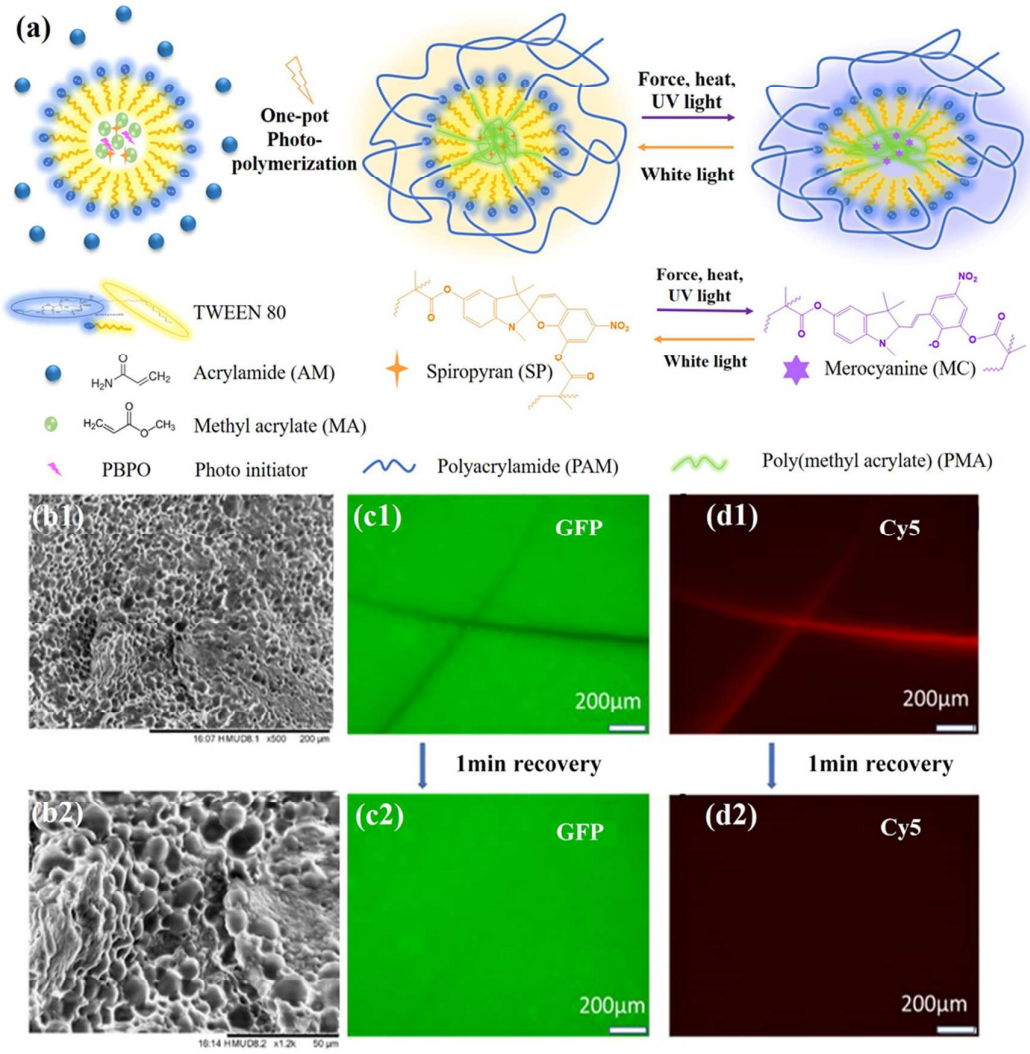

Figure 3. Visual inspection of mechanical properties of poly(AM-*co*-MA/SP) hydrogels by (a) knotted stretching; (b) weight lifting, and (c) crack propagation resistance.

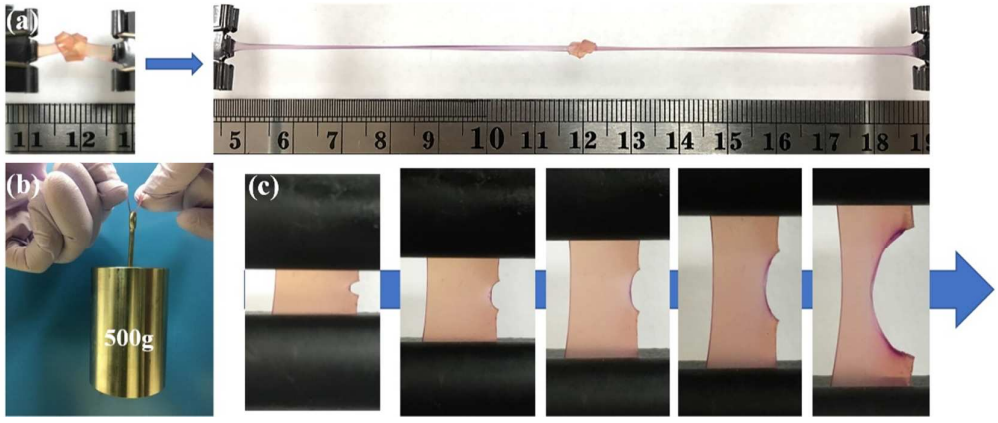

Figure 4. Mechanical properties of as-prepared poly(AM-*co*-MA/SP) hydrogels as a function of (a-b) crosslinkers, (c) MA:AM ratios, and (d) SP concentrations. (e-f) the corresponding color change of hydrogels in response to the external force during the same tensile stress-strain tests in (c-d).

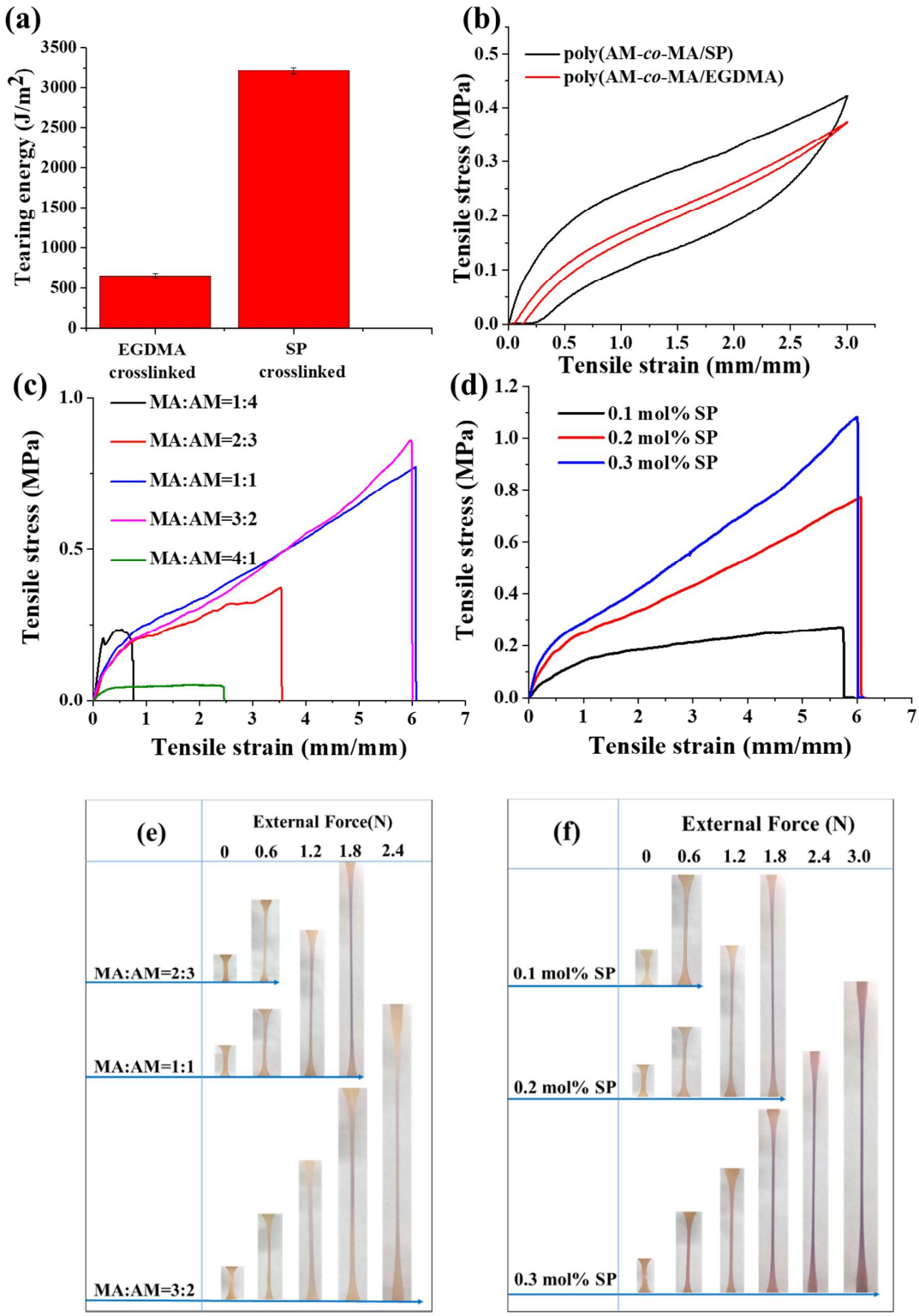

Figure 5. Schematic structural deformation process of poly(AM-*co*-MA/SP) hydrogels with low or high MA:AM concentration ratio.

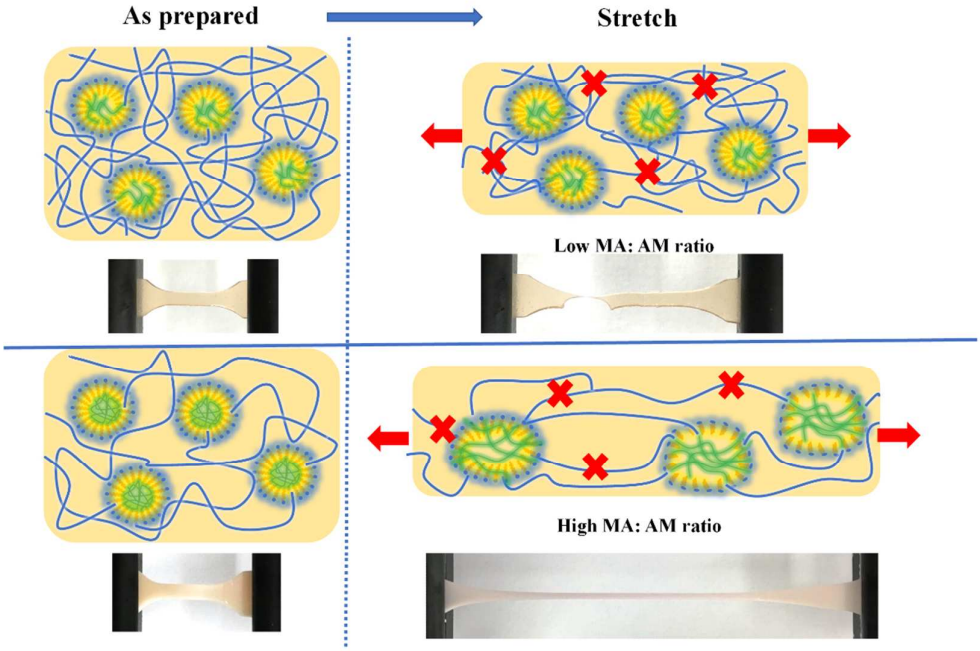

Figure 6. Swelling behaviors of poly(AM-*co*-MA/SP) hydrogels as a function of (a) MA:AM ratios and (b) SP concentrations including (a1, b1) side-by-side image comparison between as-prepared and swollen gels; (a2, b2) swelling ratios, and (a3, b3) tensile properties.

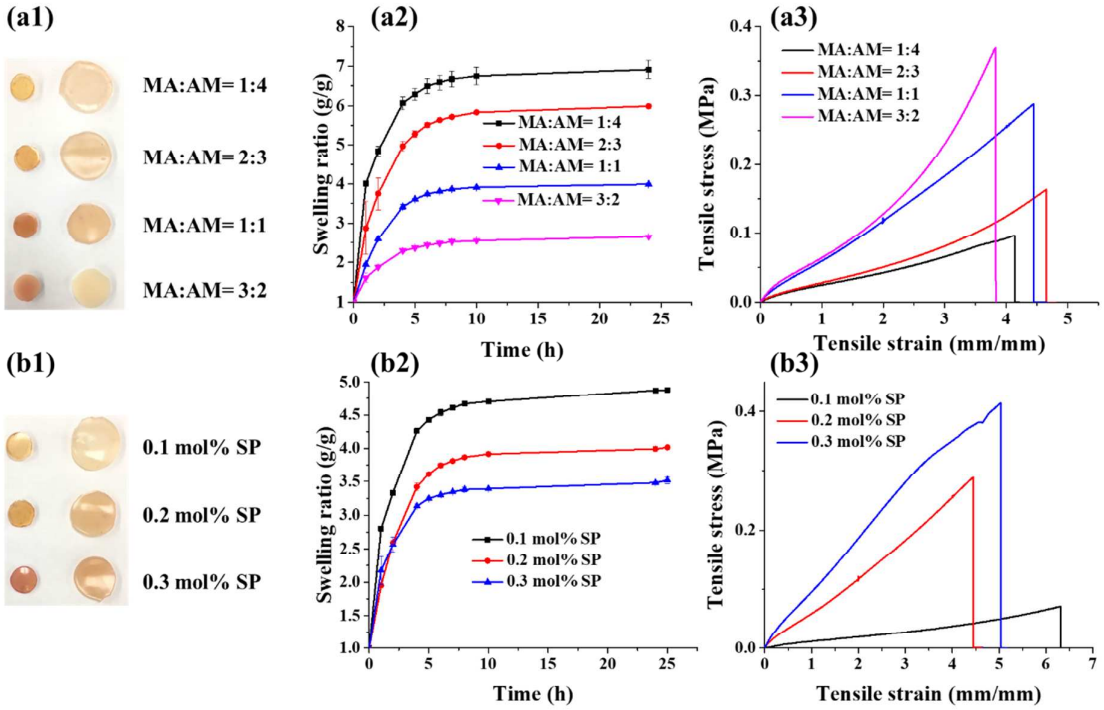

Figure 7. Reversible color and mechanical changes of poly(AM-*co*-MA/SP) hydrogels using cyclic loading-unloading tests, as demonstrated by (a) visual inspection of color change and recovery; (b) cyclic stress-strain curves; and (c) elastic modulus (stiffness) and energy loss (toughness) recovery.

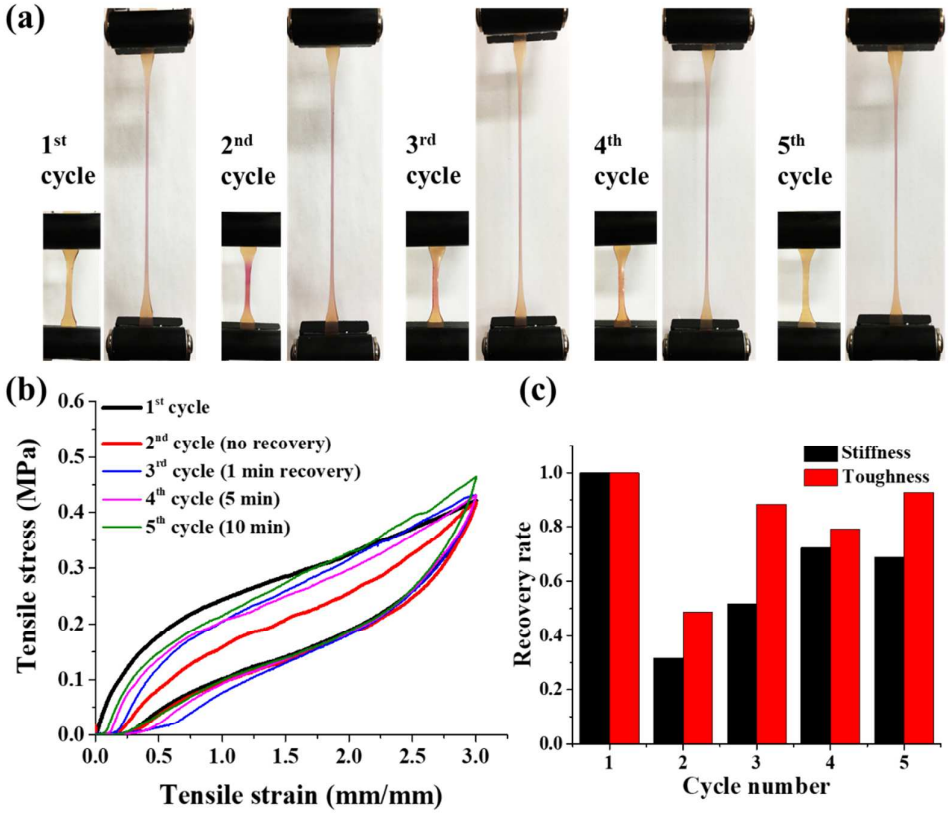

Figure 8. Comparison of mechanical properties between (a) white light- and (b) UV-treated poly(AM-*co*-MA/SP) hydrogels using the three cyclic loading-unloading tests, during which the exact same 1st and 2nd cycles are applied to the gel specimens, followed by the distinct 3rd cycle to treat one specimen with white-light, but another one with UV light.

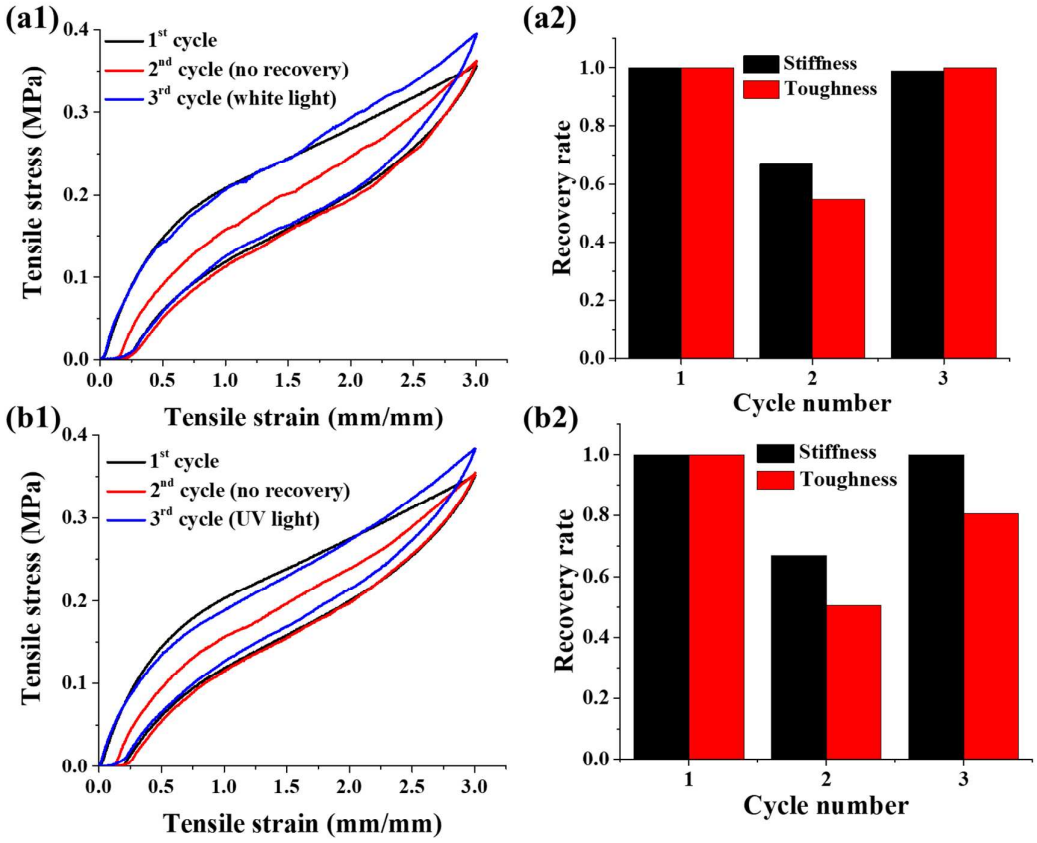

Figure 9. Reversible color change of poly(AM-*co*-MA/SP) hydrogels. (a) Visual inspection of reversible color change of poly(AM-*co*-MA/SP) hydrogels between force-, heat- and UV light-induced purple and white-light-induced yellow. (b) Color recovery pathways from purple to yellow under different external stimuli.

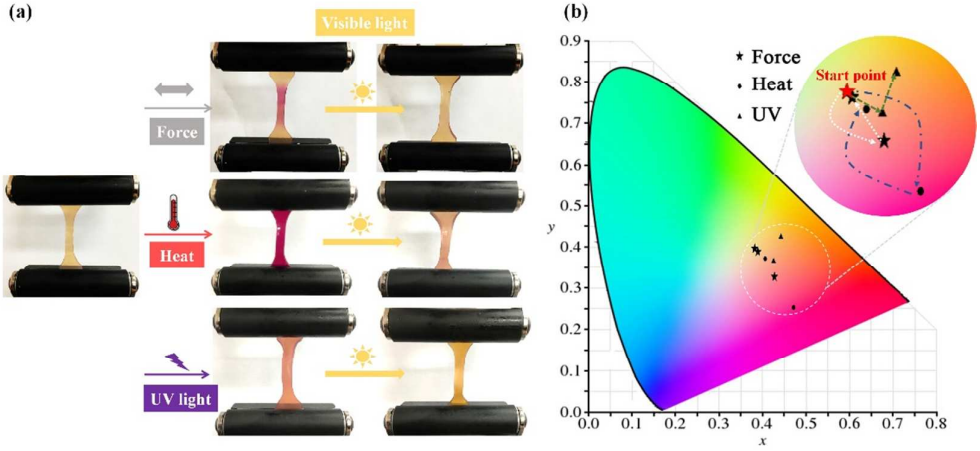

Figure 10. Reversible mechanical properties of poly(AM-*co*-MA/SP) hydrogels by three cyclic loading-unloading tested. (a) Hysteresis loop of as-prepared poly(AM-*co*-MA/SP) hydrogels in the first loading-unloading cycle as a control; (b1-b3) Comparison of hysteresis loops between force-, heat-, UV-induced deformed gels in the 2nd cycle and white-light-induced recovered gels in the 3rd cycle, and (c1-c3) the corresponding analysis for both elastic modulus (stiffness) and energy loss (toughness) recovery derived from the ratios of hysteresis loops in (b1-b3) vs. hysteresis loop in (a).

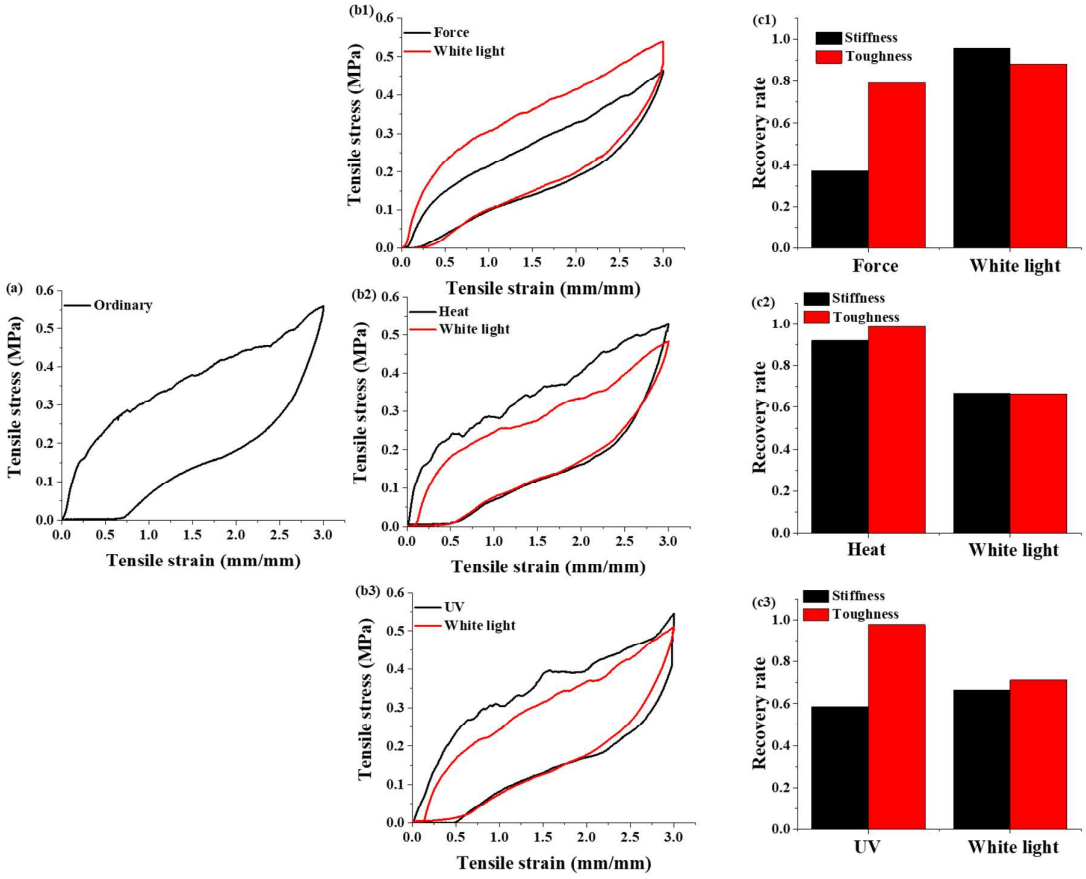

Figure 11. Poly(AM-*co*-MA/SP) hydrogel used as a strain-induced color sensor. (a) RGB color analysis for the image capture and processing procedures and (b) the strain-induced color changes in the CIE xy chromaticity diagram during the gel stretching and relaxing pathways.

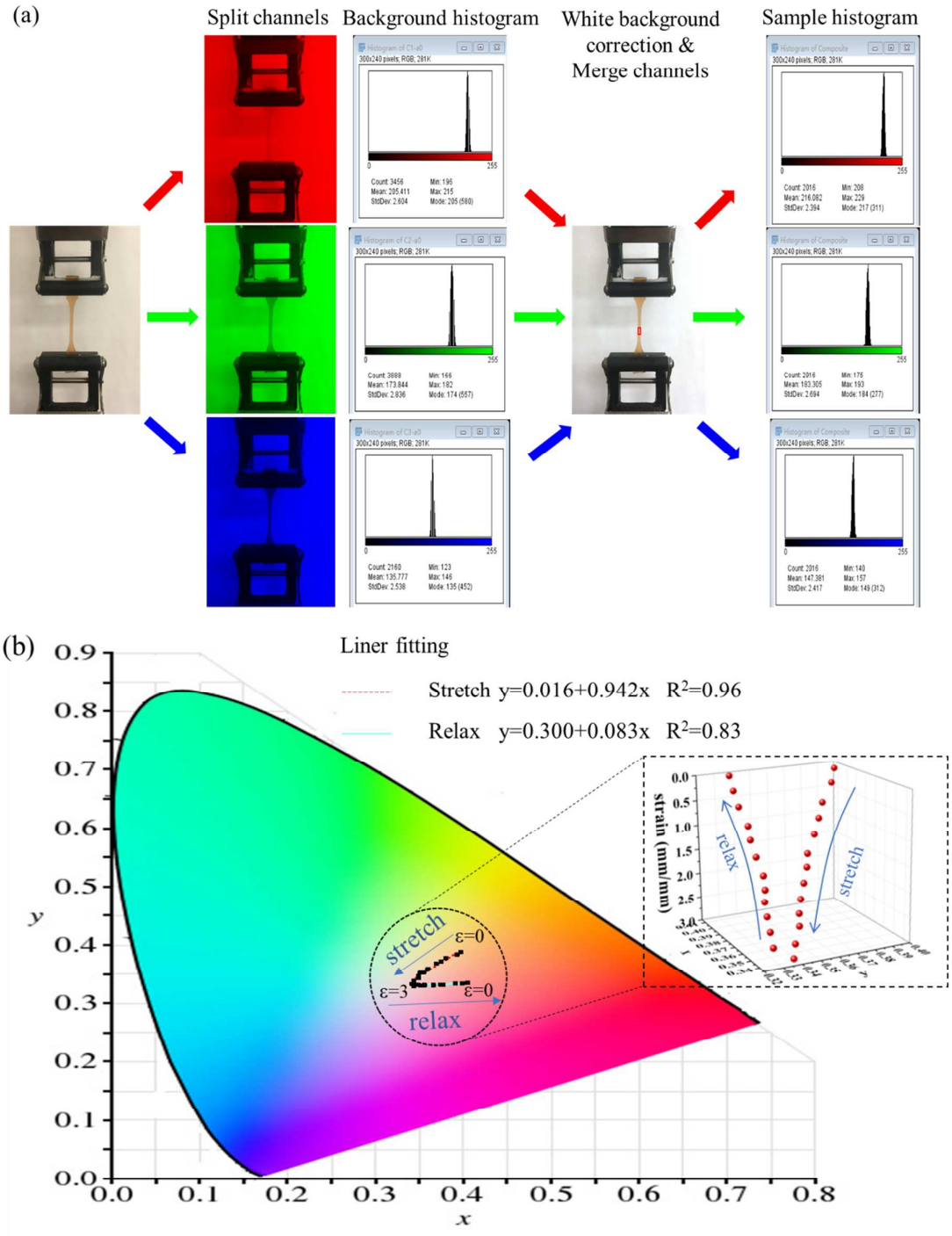

Figure 12. (a) RGB color change of poly(AM-co-MA/SP) hydrogels as a function of response time at a constant strain of ε=3. (b) Color reversibility of poly(AM-co-MA/SP) hydrogels during the fifteen loading-unloading cycles.

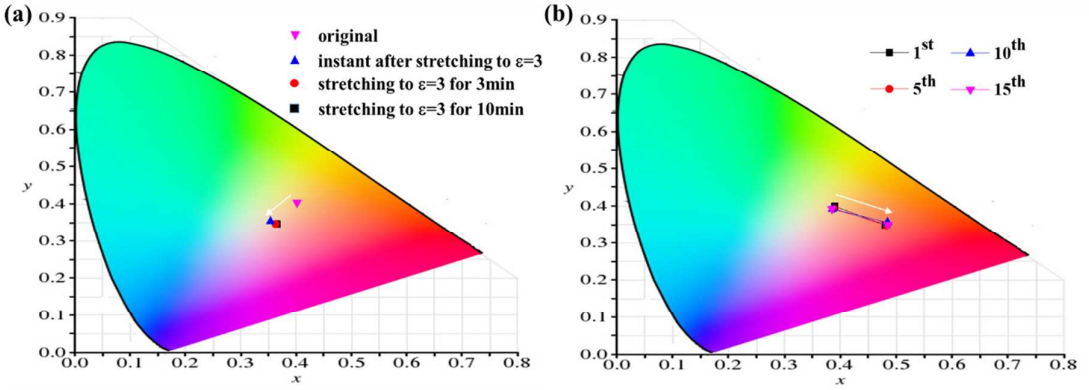

REFERENCES

1. Y. Zhao, *Macromolecules*, 2012, **45**, 3647-3657.
2. A. Koçer, M. Walko, W. Meijberg and B. L. Feringa, *Science*, 2005, **309**, 755-758.
3. W. Zhang and T. Aida, *Science*, 2012, **337**, 1462-1463.
4. D. Roy, W. L. Brooks and B. S. Sumerlin, *Chemical Society Reviews*, 2013, **42**, 7214-7243.
5. J.-F. Lutz, Ö. Akdemir and A. Hoth, *Journal of the American Chemical Society*, 2006, **128**, 13046-13047.
6. S. Dai, P. Ravi and K. C. Tam, *Soft Matter*, 2008, **4**, 435-449.
7. K. Zhou, H. Liu, S. Zhang, X. Huang, Y. Wang, G. Huang, B. D. Sumer and J. Gao, *Journal of the American Chemical Society*, 2012, **134**, 7803-7811.
8. Z. S. Siwy and S. Howorka, *Chemical Society Reviews*, 2010, **39**, 1115-1132.
9. L. Peng, A. Feng, H. Zhang, H. Wang, C. Jian, B. Liu, W. Gao and J. Yuan, *Polymer Chemistry*, 2014, **5**, 1751-1759.
10. Q. Yan, J. Yuan, Z. Cai, Y. Xin, Y. Kang and Y. Yin, *Journal of the American Chemical Society*, 2010, **132**, 9268-9270.
11. Q. Dai and A. Nelson, *Chemical Society Reviews*, 2010, **39**, 4057-4066.
12. G. Kwak, W.-E. Lee, H. Jeong, T. Sakaguchi and M. Fujiki, *Macromolecules*, 2008, **42**, 20-24.
13. J. P. Magnusson, A. Khan, G. Pasparakis, A. O. Saeed, W. Wang and C. Alexander, *Journal of the American Chemical Society*, 2008, **130**, 10852-10853.
14. S. Xiao, Y. Zhang, M. Shen, F. Chen, P. Fan, M. Zhong, B. Ren, J. Yang and J. Zheng, *Langmuir*, 2017, **34**, 97-105.
15. S. Xiao, B. Ren, L. Huang, M. Shen, Y. Zhang, M. Zhong, J. Yang and J. Zheng, *Current Opinion in Chemical Engineering*, 2018, **19**, 86-93.
16. R. T. Jakobs, S. Ma and R. P. Sijbesma, *ACS Macro Letters*, 2013, **2**, 613-616.
17. J. M. Lenhardt, A. L. Black and S. L. Craig, *Journal of the American Chemical Society*, 2009, **131**, 10818-10819.
18. C. E. Diesendruck, B. D. Steinberg, N. Sugai, M. N. Silberstein, N. R. Sottos, S. R. White, P. V. Braun and J. S. Moore, *Journal of the American Chemical Society*, 2012, **134**, 12446-12449.
19. M. M. Caruso, D. A. Davis, Q. Shen, S. A. Odom, N. R. Sottos, S. R. White and J. S. Moore, *Chemical Reviews*, 2009, **109**, 5755-5798.
20. D. A. Davis, A. Hamilton, J. Yang, L. D. Cremar, D. Van Gough, S. L. Potisek, M. T. Ong, P. V. Braun, T. J. Martínez and S. R. White, *Nature*, 2009, **459**, 68-72.
21. Y. Chen, A. Spiering, S. Karthikeyan, G. W. Peters, E. Meijer and R. P. Sijbesma, *Nature chemistry*, 2012, **4**, 559-562.
22. R. Klajn, *Chemical Society Reviews*, 2014, **43**, 148-184.
23. H. Zhang, Y. Chen, Y. Lin, X. Fang, Y. Xu, Y. Ruan and W. Weng, *Macromolecules*, 2014, **47**, 6783-6790.
24. A.-D. N. Celestine, B. A. Beiermann, P. A. May, J. S. Moore, N. R. Sottos and S. R. White, *Polymer*, 2014, **55**, 4164-4171.
25. G. R. Gossweiler, G. B. Hewage, G. Soriano, Q. Wang, G. W. Welshofer, X. Zhao and S. L. Craig, *ACS Macro Letters*, 2014, **3**, 216-219.
26. M. Li, Q. Zhang, Y.-N. Zhou and S. Zhu, *Progress in Polymer Science*, 2017, **79**, 26-39.
27. H. Chen, F. Yang, Q. Chen and J. Zheng, *Advanced Materials*, 2017, **29**, 1606900.
28. D. J. Chung, Y. Ito and Y. Imanishi, *Journal of applied polymer science*, 1994, **51**, 2027-2033.

29. S. Wu, J. Lu, F. Zeng, Y. Chen and Z. Tong, *Macromolecules*, 2007, **40**, 5060-5066.
30. L. A. Connal, G. V. Franks and G. G. Qiao, *Langmuir*, 2010, **26**, 10397-10400.
31. M. Moniruzzaman, C. Sabey and G. Fernando, *Polymer*, 2007, **48**, 255-263.
32. J. Ratner, N. Kahana, A. Warshawsky and V. Krongauz, *Industrial & engineering chemistry research*, 1996, **35**, 1307-1315.
33. H. R. Allcock and C. Kim, *Macromolecules*, 1991, **24**, 2846-2851.
34. Y. J. Oh, J. A. Nam, A. Al□Nahain, S. Lee, I. In and S. Y. Park, *Macromolecular rapid communications*, 2012, **33**, 1958-1963.
35. M. Li, Q. Zhang and S. Zhu, *Polymer*, 2016, **99**, 521-528.
36. Q. Wang, G. R. Gossweiler, S. L. Craig and X. Zhao, *Nature communications*, 2014, **5**, 4899.
37. G. I. Peterson, M. Yurtoglu, M. B. Larsen, S. L. Craig, M. A. Ganter, D. W. Storti and A. J. Boydston, *Rapid Prototyping Journal*, 2015, **21**, 520-527.
38. J. Ter Schiphorst, M. Van Den Broek, T. De Koning, J. Murphy, A. Schenning and A. Esteves, *Journal of Materials Chemistry A*, 2016, **4**, 8676-8681.
39. Z. Qiu, H. Yu, J. Li, Y. Wang and Y. Zhang, *Chemical Communications*, 2009, **23**, 3342-3344.
40. D. J. Cornwell and D. K. Smith, *Materials Horizons*, 2015, **2**, 279-293.
41. Z. Sun, S. Liu, K. Li, L. Tan, L. Cen and G. Fu, *Soft matter*, 2016, **12**, 2192-2199.
42. C. K. Lee, B. A. Beiermann and M. N. Silberstein, *Macromolecules*, 2013, **46**, 3746-3752.
43. X. Fang, H. Zhang, Y. Chen, Y. Lin, Y. Xu and W. Weng, *Macromolecules*, 2013, **46**, 6566-6574.
44. S. L. Potisek, D. A. Davis, N. R. Sottos, S. R. White and J. S. Moore, *Journal of the American Chemical Society*, 2007, **129**, 13808-13809.
45. J. Guo, X. Liu, N. Jiang, A. K. Yetisen, H. Yuk, C. Yang, A. Khademhosseini, X. Zhao and S. H. Yun, *Advanced Materials*, 2016, **28**, 10244-10249.